E6C15 (E = Si–Pb): polycyclic aromatic compounds with three planar tetracoordinate carbons

Luis Leyva-Parra, Diego Inostroza, Alejandro Vásquez-Espinal, Julia Contreras-García, Zhong-Hua Cui, Sudip Pan, Venkatesan S Thimmakondu, William Tiznado

COMMUNICATION

E_6C_{15} (E = Si-Pb): Polycyclic Aromatic Compounds with Three planar Tetracoordinate Carbons

Received 00th January 20xx,
Accepted 00th January 20xx

DOI: 10.1039/x0xx00000x

Diego Inostroza,[a,b] Luis Leyva-Parra[a,b], Alejandro Vásquez-Espinal[c] ,Julia Contreras-García[d], Zhong-hua Cui,[e,f] Sudip Pan,[g,*] Venkatesan S. Thimmakondu ,[h,*] and William Tiznado.[a,*]

A systematic exploration of the potential energy surface reveals two global minima with three planar tetra coordinate carbons (ptCs) and two global minima with three quasi-ptCs for E_6C_{15} (E = Si-Pb) combinations. These consist of aromatic polycyclic templates suitable to further design different materials without hindering the ptC texture.

In 1970, Hoffmann and co-workers argued that incorporating π-acceptor/σ-donor ligands could reduce stereomutation barriers involving a planar tetracoordinate carbon (ptC) transition state (TS) for some tetrahedral carbon compounds.[1] The approach was successfully adopted by the group of Schleyer to predict the first ptC local minimum structure.[2] In 1977, the V_2(2,6-dimethoxyphenyl)$_4$ complex was characterized via X-ray diffraction,[3] being the first experimental ptC example, although this was not recognized for more than ten years. These findings stimulated numerous pieces of research looking for ways to prepare stable "antivan't Hoff/LeBel compounds," i.e., molecular substances containing tetracoordinate carbon in a non-tetrahedral coordination geometry.

In the last 50 years, significant progress has been made in synthesizing and theoretically predicting numerous ptC compounds.[4–10] Most recently, the world of planar hypercoordinate carbon was extended to higher carbon coordination (penta[11–20] and hexacoordinate[21–24]). The invocation of the chemical bonding concept is crucial for understanding the construction principles and searching to maximize stabilizing interactions in favor of these structures. Thus, several strategies were compiled, some of which take advantage of π- and σ-bond delocalization (i.e., aromaticity, resonance).

Here we report the E_6C_{15} (E = Si, Ge, Sn) putative global minima (GM), which consists of a C_{15} tetracyclic structure with three ptC units. To design these systems, we replaced each of the three neighboring protons of the $C_{15}H_9^{3-}$ moiety with two E^{2+} ligands (Scheme 1). $C_{15}H_9^{3-}$ was designed from **1** ([6]radialenes), see Scheme 1 (left), searching for a template with three pentagonal aromatic rings suitable to stabilize ptCs.[19,25–27] Note that even in very small systems, the group 14 elements favors ptCs.[28–30]

A systematic exploration of the potential energy surfaces (PESs) using the AUTOMATON program[31,32] and atomic permutations starting from known templates (Supporting Information) allowed us to identify the relevant minimum energy structures. The initial screening (singlet and triplet states) was done at the PBE0[33]-D3[34] /SDDALL[35] level. Then, low-lying energy isomers (< 30.0 kcal·mol^{-1} above the putative GM) were re-minimized at the PBE0-D3/Def2-TZVP[36] level and harmonic frequency calculations to verify they are true minima on the PES. All these calculations were performed using the Gaussian16 program.[37]

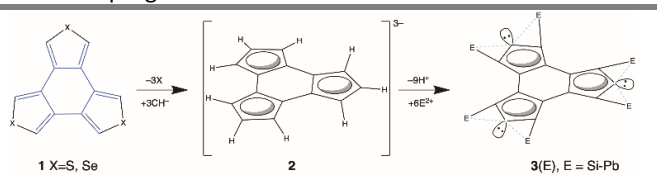

Scheme 1. Design of E_6C_{15} ptC systems starting from the [6]radialenes benzo[1,2-c :3,4-c':5,6-c'']trithiophene or benzo[1,2-c:3,4-c':5,6-c'']triselenophene (**1**) to build $C_{15}H_9^{3-}$ (**2**) and finally the ptC candidate compounds **3**(E).

The E_6C_{15} lowest energy structures are reported in Figure 1. Remarkably, compounds **3**(Si) and **3**(Ge) are the putative GM adopting a planar D_{3h} symmetry, while the nearest energy isomer, also with three ptCs, lies at 8.2 and 2.8 kcal·mol^{-1} above the putative GM (Figs. S1-S2). In the heavier congeners (Sn and Pb), the **4**(E) isomer is revealed as the putative GM, with a C_{15} backbone analogous to that of the **3**(E) but bent due to the connection of the pentagonal rings by E-bridging bonds.

[a] *Computational and Theoretical Chemistry Group, Departamento de Ciencias Químicas, Facultad de Ciencias Exactas, Universidad Andres Bello, República 498, Santiago, Chile. E-mail: wtiznado@unab.cl*
[b] *Doctorado en Fisicoquímica Molecular, Facultad de Ciencias Exactas, Universidad Andres Bello, República 275, Santiago, Chile.*
[c] *Química y Farmacia, Facultad de Ciencias de la Salud, Universidad Arturo Prat, Casilla 121, Iquique 1100000, Chile*
[d] *Sorbonne Universités and CNRS, Laboratoire de Chimie Théorique (LCT), 75005 Paris, France.*
[e] *Institute of Atomic and Molecular Physics, Jilin University, Changchun 130023, China.*
[f] *Key Laboratory of Physics and Technology for Advanced Batteries (Ministry of Education), Jilin University, Changchun 130023, China.*
[g] *Fachbereich Chemie,Philipps-Universitt Marburg Hans-Meerwein-Straße,35043 Marburg, Germany. E-mail: pans@chemie.uni-marburg.de*
[h] *Department of Chemistry and Biochemistry, San Diego State University, San Diego, CA, 92182-1030 USA E-mail: vthimmakondusamy@sdsu.edu*

Noteworthy, **4**(E) isomers exhibit three quasi-planar tetracoordinate carbons. Thus, we identified four new putative GMs, two of them with three ptCs each, and the other two with three quasi-ptCs each. The putative GM's HOMO-LUMO energy gaps are relatively high, varying between 2.13 and 4.03 eV. Relevant low-lying isomers of E_6C_{15} (E = Si-Pb) are listed in Figs. S1-S4 of supporting information. Isomerization energy decomposition analysis (IEDA)[38] explains these preferences. Essentially, the distortion energy of the C_{15} backbone is lower as E is heavier, allowing a better stabilization of **4**(E) for E=Sn and Pb concerning the **3**(E) structures (a detailed explanation is given in the supporting information).

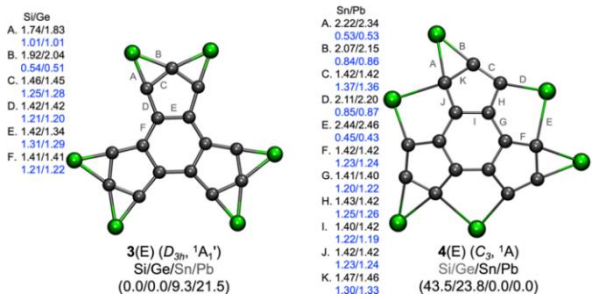

Figure 1. Lowest energy structures of E_6C_{15} at PBE0-D3/def2-TZVP level (relative energies in kcal·mol^{-1}, including zero-point energy (ZPE) corrections). The bond length in Å (black) and *WBI* values (blue) at PBE0-D3/def2-TZVP level.

The C–C distances lie within those of single and double bonds (1.41-1.47 Å), which is consistent with the delocalized nature of the bonding (*vide infra*). There are two different kinds of C-E bonds, one being shorter than a single bond and another slightly longer than it. The corresponding Wiberg bond index (*WBI*) [39] values also agree with the bond distances (see Fig. 1). The E atoms in the putative GM bear positive natural charges, computed by natural population analysis (NPA),[40] ranging within 0.87-0.97 |e|, neutralized by negative charges distributed on the carbons bonded to the E atoms (see Figs. S5-S6), which is consistent with the difference in C-E electronegativity. For comparative purposes, 3(E) and 4(E) structures have also been optimized at the ωB97XD[41]/Def2-TZVP and MP2[42]/Def2-TZVP levels, and *WBI* values have also been computed at these levels. Figures S7 and S8, show minimal changes in structural and bond order properties regarding PBE0-D3/Def2-TZVP level.

The adaptive natural density partitioning (AdNDP) method,[43,44] which is an extension of natural bond orbital (NBO) analysis, allows interpreting chemical bonding in terms of two-electron n-center bonds (nc-2e), with n ranging from one to the total number of atoms in the molecule, recovering Lewis's elements (lone pairs and 2c-2e bonds) and nc-2e delocalized bonds. The bonding of **3**(Si) and **3**(Ge) are similar, also **4**(Sn) and **4**(Pb), thus, we will discuss the **3**(Si), and **4**(Sn) results as representative cases. Figure 2 shows the AdNDP localization of the 42 valence electron pairs in **3**(Si). Six lone pairs are recovered (one on each Si), and 18 2c-2e σ-bonds connect the C_{15} backbone. The six Si are linked to the C_{15} backbone by six 2c-2e C-Si σ-bonds and three 3c-2e Si-ptC-Si σ-bonds. This explains why there are one short and one longer C-Si bond distances. Also, nine delocalized π-bonds, consisting of six distributed on the pentagonal rings (4c-2e) and three on the central hexagonal ring (4c-2e), complete the bonding picture of **3**(Si). It is essential to highlight the presence of delocalized bonds, three isolated σ (3c-2e) bonds in the outer Si-C-Si moiety, and nine π (4c-2e) bonds, among which six are distributed on the pentagonal ring and connected Si centers. The remaining three bonds are delocalized over the hexagonal ring. Thus, evoking Hückel's 4n+2 rule, this system should be aromatic. In the **4**(Sn) and **4**(Pb) isomers, the bonding pattern is also very similar to that of **3**(E), only now the quasi-ptC corresponds to the carbons connecting the pentagonal rings through 2c-2e C-E σ-bonds (Fig. S10).

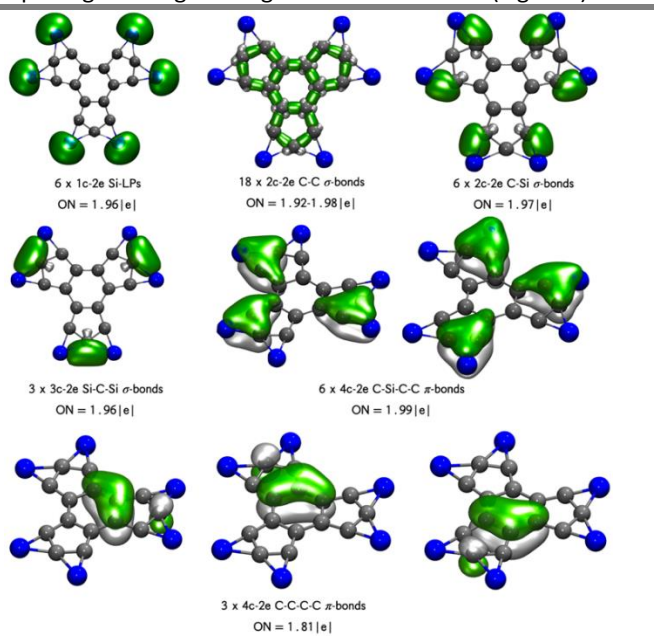

Figure 2. AdNDP analysis of **3**(Si) system (D_{3h}-Si_6C_{15}). ON stands for occupation number. Carbon=gray, silicon=blue.

To further assess aromaticity, both qualitatively and quantitatively, we computed current densities using the GIMIC program,[45,46] which employs the gauge-including atomic orbital (GIAO)[47] method. To visualize current pathways, we used Paraview 5.10.0 software. Fig. 3 shows the ring current circuits and their magnitudes according to the ring current strength (RCSs). These circuits are identified by analyzing RCS profiles of different integration planes, following a previously proposed strategy,[48–50] as detailed in Figs. S11-S14. In this analysis, diatropic (aromatic) and paratropic (antiaromatic) currents turn clockwise and counterclockwise, respectively. A positive (diatropic) and negative (paratropic) RCS sign correspond to aromatic and anti-aromatic circuits, respectively. Besides, the RCS values close to zero suggest a non-aromatic character.[49]

As seen in Fig. 3, **3**(Si) exhibits two global concentric diatropic ring currents, both of medium to low intensity, 5.6 (the outermost) and 3.3 nA·T^{-1} (the innermost), resulting in a total of 8.9 nA·T^{-1}, which is significant when compared to that of benzene at the same level (11.8 nA·T^{-1}). Three local ring currents are also revealed, with RCS values of 6.7 nA·T^{-1}, around the ptCs. As seen in Figs. S15 and S16, this local ring current is the most evident at the molecular plane, supporting a σ-aromatic nature and would be connected to the 3c-2e Si-ptC-Si

σ-bond detected in the AdNDP analysis. Also, three horseshoe-shaped currents are distributed around the C-ptC-C fragments, with an RCS of 4.1 nA·T^{-1}. The central C_6 ring also exhibits a diatropic ring current (RCS = 4.4 nA·T^{-1}) and an innermost paratropic ring current (RCS = –2.9 nA·T^{-1}). While the pentagonal rings only exhibit local paratropic ring currents with marginal RCS values of -1.3 nA·T^{-1}. The magnetic behavior of **3**(Ge) is very similar to **3**(Si). Therefore, it could be concluded that **3**(Si) and **3**(Ge) exhibit global aromaticity, local marginal aromaticity in the central C_6 ring, and local σ-aromaticity in the E-ptC-E fragment.

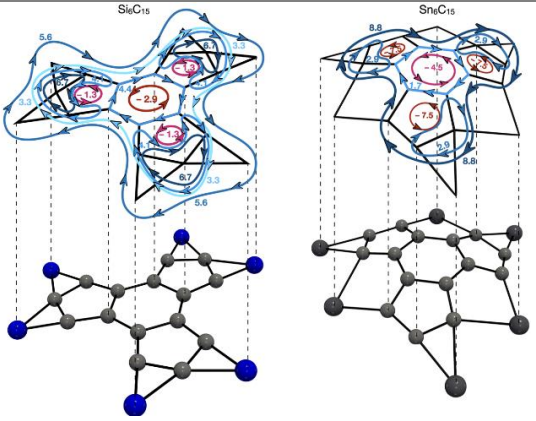

Figure 3. Identified ring current circuits in **3**(Si) (left) and **4**(Sn) (right) systems. Each circuit's RCS value is reported in nA·T^{-1}

System **4**(Sn) exhibits ring current patterns quite similar to **3**(E): one global diatropic ring current, with an RCS value of 8.8 nA·T^{-1} [1] (see Fig. 3). Three local ring currents around the ptCs with marginal RCS values (2.3 nA·T^{-1}). The latter ring currents are more evident on the plane close to the ptCs and would be associated with the 3c-2e Sn-ptC-Sn σ-bonds (see Figs. S17-S18). The central C_6 ring exhibits a weak diatropic ring current with an RCS of 1.7 nA·T^{-1} and an innermost paratropic ring current with an RCS value of –4.5 nA·T^{-1}. While the outer pentagonal rings only exhibit local paratropic ring currents with RCS values of -7.5 nA·T^{-1}. **4**(Pb) also shows similar magnetic properties. Therefore, it could be concluded that **4**(Sn) and **4**(Pb) are globally aromatic, slightly local antiaromatic in the central C_6 ring, locally antiaromatic (in the peripheral C_5 rings), and locally σ-aromatic due to the 3c-2e E-ptC-E bonds.

The AdNDP analysis shows that each E center possesses a lone pair of electrons. Therefore, E might be considered one of the key centers for reactivity toward electrophiles. We studied the possibility of forming a Lewis acid-base complex taking BH_3 as Lewis acid. Fig. 4 shows the minimum energy geometries of **3**(Si)-$(BH_3)_6$ and **3**(Ge)-$(BH_3)_6$ complexes. The complex formation is exergonic in nature at room temperature, having a bond dissociation free energy, ΔG^{298K} of 16.0 (E = Si) and 8.8 (E = Ge) kcal·mol^{-1} per BH_3. As expected, the resulting complexes are electronically more stable and less reactive than bare **3**(Si) and **3**(Ge), which can be understood by the improvement in $\Delta_{H\text{-}L}$ values (by 0.39 and 0.36 eV, respectively). Another way to protect a compound from reacting is to block the reactive center by forming a host-guest complex. We found that [12]cycloparaphenylene ([12]CPPs) has the perfect size to accommodate **3**(Si) and **3**(Ge) and the encapsulation process is exergonic in nature by ΔG^{298K} = –7.1 and –9.7 kcal·mol^{-1}, respectively. We further studied the possibility of forming a sandwich complex between coronene and **3**(Si). As shown in Fig. 4, the resulting complex is highly stable against dissociation. Therefore, contrary to the many reported ptC systems, the ones reported here, having aromatic polycyclic templates, can be used to further design different materials without hampering ptC texture. We have also verified that the 3(Si) dimer formation in the parallel displaced configuration is an exergonic process (ΔG^{298K} = –10.4 kcal·mol^{-1}); where the ptCs are only marginally away from the plane, see Figure S19.

Conclusions

To summarize, GM polycyclic structures with the formula E_6C_{15} (E = Si-Pb) with three ptCs or three quasi-ptCs each are revealed. It is found that for E = Si and Ge, the putative GM consist of three ptC centers. In contrast, for E = Sn and Pb, because of the large size, the most stable isomer has a bowl-shaped structure with three quasi-ptCs. Chemical bonding analysis reveals the presence of three delocalized E-ptC-E 3c-2e σ-bonds and nine delocalized π-bonds, supporting an aromatic character according to Hückel's 4n+2 rule. The magnetically induced current density analysis reveals global and local ring current circuits supporting these species' global and local aromatic character. These title systems can also be used as a partner to form supramolecular complexes with coronene or [12]CPP without hampering ptC moieties. This could also pave the way for their large-scale syntheses.

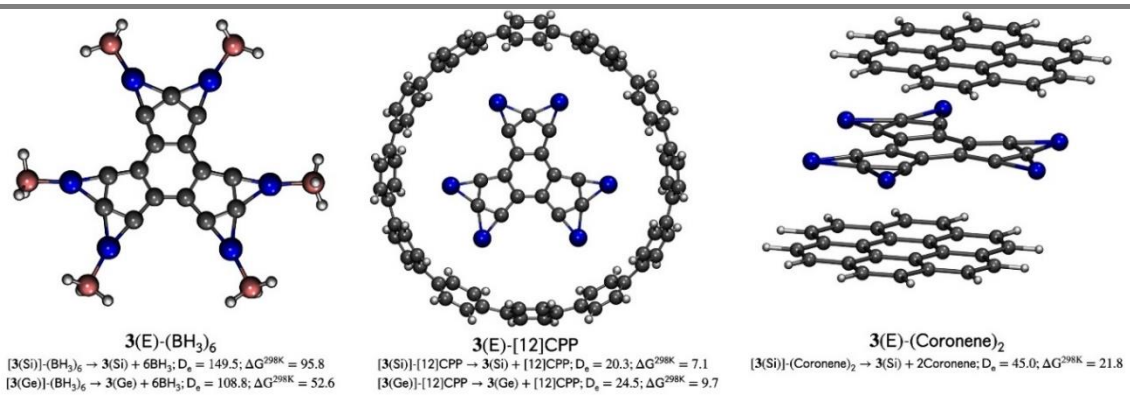

Fig. 4 The minimum energy geometries of **3**(Si)/**3**(Ge)-$(BH_3)_6$, **3**(Si)/**3**(Ge)-[12]CPP, and **3**(Si)-$(Coronene)_2$ complexes at the PBE0-D3/def2-TZVP level, except for sandwich complex for which def2-SVP is used. The bond dissociation energies at 0 K (De) and 298 K, including thermal correction and entropy factors (ΔG^{298K}), are given in kcal·mol^{-1}.

This work was supported by the financial support of the National Agency for Research and Development (ANID) through FONDECYT projects 1211128 (W.T.) and 1221019 (A.V.-E.) and National Agency for Research and Development (ANID)/Scholarship Program/BECAS DOCTORADO NACIONAL/2019-21190427 (D.I.) and 2020-21201177 (L.L-P.). and ECOS program C17E09. Powered@NLHPC: This research was partially supported by the supercomputing infrastructure of the NLHPC (ECM-02). Computational support provided at SDSU (for V.S.T) is gratefully acknowledged.

Conflicts of interest

There are no conflicts to declare.

Notes and references

1 R. Hoffmann, R. W. Alder and C. F. Wilcox, *J. Am. Chem. Soc.*, 1970, **92**, 4992–4993.
2 J. B. Collins, J. D. Dill, E. D. Jemmis, Y. Apeloig, P. v. Schleyer, R. Seeger and J. A. Pople, *J. Am. Chem. Soc.*, 1976, **98**, 5419–5427.
3 F. A. Cotton and M. Millar, *J. Am. Chem. Soc.*, 1977, **99**, 7886–7891.
4 G. Erker, *Comment Inorg. Chem.* 1992, **13**, 111–131.
5 D. Röttger and G. Erker, *Angew. Chem. Int. Edit.*, 1997, **36**, 812–827.
6 1. W. Siebert and A. Gunale, *Chem. Soc. Rev.*, 1999, **28**, 367-371.
7 R. Keese, *Chem. Rev.*, 2006, **106**, 4787–4808.
8 G. Merino, M. A. Méndez-Rojas, A. Vela and T. Heine, *J. Comput. Chem.*, 2006, **28**, 362–372.
9 X.-yong Zhang and Y.-hong Ding, *Comput. Theor. Chem.*, 2014, **1048**, 18–24.
10 X. Li, H.-F. Zhang, L.-S. Wang, G. D. Geske and A. I. Boldyrev, *Angew. Chem. Int. Edit.*, 2000, **39**, 3630–3632.
11 Z.-X. Wang and P. von Schleyer, *Science*, 2001, 292, 2465–2469.
12 Y. Wang, F. Li, Y. Li and Z. Chen, *Nat. Commun.*, 2016, **7**, 11488.
13 S. Pan, J. L. Cabellos, M. Orozco-Ic, P. K. Chattaraj, L. Zhao and G. Merino, *Phys. Chem. Chem. Phys.*, 2018, **20**, 12350–12355.
14 Y. Pei, W. An, K. Ito, P. von Schleyer and X. C. Zeng, *J. Am. Chem. Soc.*, 2008, **130**, 10394–10400.
15 V. Vassilev-Galindo, S. Pan, K. J. Donald and G. Merino, *Nat. Rev. Chem.*, 2018, **2**.
16 R. Grande-Aztatzi, J. L. Cabellos, R. Islas, I. Infante, J. M. Mercero, A. Restrepo and G. Merino, *Phys. Chem. Chem. Phys.*, 2015, **17**, 4620–4624.
17 X.-F. Zhao, J.-H. Bian, F. Huang, C. Yuan, Q. Wang, P. Liu, D. Li, X. Wang and Y.-B. Wu, *RSC Adv*, 2018, **8**, 36521–36526.
18 Z.-hua Cui, V. Vassilev-Galindo, J. Luis Cabellos, E. Osorio, M. Orozco, S. Pan, Y.-hong Ding and G. Merino, *Chem. Commun.*, 2017, **53**, 138–141.
19 O. Yañez, R. Báez-Grez, J. Garza, S. Pan, J. Barroso, A. Vásquez-Espinal, G. Merino and W. Tiznado, *ChemPhysChem*, 2019, **21**, 145–148.
20 L. Leyva-Parra, L. Diego, D. Inostroza, O. Yañez, R. Pumachagua-Huertas, J. Barroso, A. Vásquez-Espinal, G. Merino and W. Tiznado, *Chem-Eur J.*, 2021, **27**, 16701–16706.
21 Y.-B. Wu, Y. Duan, G. Lu, H.-G. Lu, P. Yang, P. von Schleyer, G. Merino, R. Islas and Z.-X. Wang, *Phys. Chem. Chem. Phys.*, 2012, **14**, 14760–14763.
22 K. Exner and P. von Schleyer, *Science*, 2000, **290**, 1937–1940.
23 L. Leyva-Parra, L. Diego, O. Yañez, D. Inostroza, J. Barroso, A. Vásquez-Espinal, G. Merino and W. Tiznado, *Angew. Chem. Int. Edit.*, 2021, **60**, 8700–8704.
24 Y. Li, Y. Liao and Z. Chen, *Angew. Chem. Int. Edit.*, 2014, **126**, 7376–7380.
25 O. Yañez, A. Vásquez-Espinal, R. Pino-Rios, F. Ferraro, S. Pan, E. Osorio, G. Merino and W. Tiznado, *Chem. Commun.*, 2017, **53**, 12112–12115.
26 O. Yañez, A. Vásquez-Espinal, R. Báez-Grez, W. A. Rabanal-León, E. Osorio, L. Ruiz and W. Tiznado, *New J. Chem.*, 2019, **43**, 6781–6785.
27 L. Leyva-Parra, D. Inostroza, O. Yañez, J. C. Cruz, J. Garza, V. García and W. Tiznado, *Atoms*, 2022, **10**, 27.
28 P. Das, M. Khatun, A. Anoop and P. K. Chattaraj, *Phys. Chem. Chem. Phys.*, 2022, **24**, 16701–16711.
29 P. Das and P. K. Chattaraj, *Atoms*, 2021, **9**, 65.
30 P. Das and P. K. Chattaraj, *J. Comput. Chem.*, 2022, **43**, 894–905.
31 O. Yañez, R. Báez-Grez, D. Inostroza, W. A. Rabanal-León, R. Pino-Rios, J. Garza and W. Tiznado, *J. Chem. Theory Comput.*, 2019, **15**, 1463–1475.
32 O. Yañez, D. Inostroza, B. Usuga-Acevedo, A. Vásquez-Espinal, R. Pino-Rios, M. Tabilo-Sepulveda, J. Garza, J. Barroso, G. Merino and W. Tiznado, *Theor. Chem. Acc.*, 2020, **139**, 41.
33 C. Adamo and V. Barone, *J. Chem. Phys.*, 1999, **110**, 6158–6170.
34 S. Grimme, J. Antony, S. Ehrlich and H. Krieg, *J. Chem. Phys.*, 2010, **132**, 154104.
35 P. Fuentealba, L. von Szentpaly, H. Preuss and H. Stoll, *J. Phys. B: At. Mol.*, 1985, **18**, 1287–1296.
36 F. Weigend and R. Ahlrichs, *Phys. Chem. Chem. Phys.*, 2005, **7**, 3297-3305.
37 M. J. Frisch, et. Gaussian 16, Revision B.01, *Gaussian, Inc.*, Wallingford CT, 2016.
38 M. Contreras, E. Osorio, F. Ferraro, G. Puga, K. J. Donald, J. G. Harrison, G. Merino and W. Tiznado, *Chem-Eur J.*, 2013, **19**, 2305–2310.
39 K. B. Wiberg, *Tetrahedron*, 1968, **24**, 1083–1096.
40 A. E. Reed, R. B. Weinstock and F. Weinhold, *J. Chem. Phys.*, 1985, **83**, 735–746.
41 J.-D. Chai and M. Head-Gordon, *Phys. Chem. Chem. Phys.*, 2008, **10**, 6615–6620.
42 M. Head-Gordon, J. A. Pople and M. J. Frisch, *Chem. Phys. Lett.*, 1988, **153**, 503–506.
43 D. Y. Zubarev and A. I. Boldyrev, *Phys. Chem. Chem. Phys.*, 2008, **10**, 5207–5217.
44 D. Y. Zubarev and A. I. Boldyrev, *J. Org. Chem.*, 2008, **73**, 9251–9258.
45 H. Fliegl, S. Taubert, O. Lehtonen and D. Sundholm, *Phys. Chem. Chem. Phys.*, 2011, **13**, 20500–20518.
46 J. Jusélius, D. Sundholm and J. Gauss, *J. Chem. Phys.*, 2004, **121**, 3952–3963.
47 K. Wolinski, J. F. Hinton and P. Pulay, *J. Am. Chem. Soc.*, 1990, **112**, 8251–8260.
48 D. Sundholm, R. J. Berger and H. Fliegl, *Phys. Chem. Chem. Phys.*, 2016, **18**, 15934–15942.
49 D. Sundholm, H. Fliegl and R. J. F. Berger, *WIRES Comput. Mol. Sci.*, 2016, **6**, 639–678.
50 D. Inostroza, V. García, O. Yañez, J. J. Torres-Vega, A. Vásquez-Espinal, R. Pino-Rios, R. Báez-Grez and W. Tiznado, *New J. Chem.*, 2021, **45**, 8345–8351.

